Broadband high dynamic range fiber optic link based on a dual-polarization modulator

Zheng, Ruiqi; Chan, Erwin H.W.; Wang, Xudong; Feng, Xinhuan; Guan, Bai Ou

Published in:
Optics Express

DOI:
10.1364/OE.27.004734

Published: 18/02/2019

Document Version
Publisher's PDF, also known as Version of record

Research Article | Vol. 27, No. 4 | 18 Feb 2019 | OPTICS EXPRESS 4734
Optics EXPRESS

Broadband high dynamic range fiber optic link based on a dual-polarization modulator

RUIQI ZHENG,[1] ERWIN H. W. CHAN,[2] XUDONG WANG,[1,*] XINHUAN FENG,[1] AND BAI-OU GUAN[1]

[1]*Guangdong Provincial Key Laboratory of Optical Fiber Sensing and Communications, Institute of Photonics Technology, Jinan University, Guangzhou 510632, China*
[2]*College of Engineering, IT and Environment, Charles Darwin University, Darwin NT 0909, Australia*
**txudong.wang@email.jnu.edu.cn*

Abstract: This paper presents a simple, linearized fiber-optic link that is capable of realizing a high spurious free dynamic range (SFDR) at different input RF signal frequencies without the need of readjusting system parameters. The link is based on a commercial dual-polarization modulator followed by a linear polarizer. The third-order nonlinearity at the third-order intermodulation distortion frequency can be cancelled by designing the angle of the linear polarizer. No electrical component is involved in the linearization process. The high SFDR performance is theoretically analyzed, simulated using photonic simulation software, and experimentally verified. Experimental verification of the dual-polarization modulator-based linearized fiber-optic link shows that a high SFDR of more than 124 dB·Hz$^{4/5}$ is obtained at different input RF signal frequencies over a 2-18 GHz bandwidth. An SFDR of 127.3 dB·Hz$^{4/5}$ is also demonstrated with the use of an optical amplifier to increase the link output average optical power, which is among the highest reported SFDRs measured in a fiber-optic link.

1. Introduction

Research on an externally modulated fiber optic link (FOL) has been conducted over the past three decades. This is driven by the fact that FOLs have many applications including cable TV distribution, real-time wideband signal transmission in radio astronomy and defense systems, and radio-over-fiber for transmission of mobile radio signals. Spurious free dynamic range (SFDR) is an important performance measure of a FOL. It is defined as the ratio of the maximum signal without creating detectable distortion to the minimum signal that is just above the system noise floor. The SFDR of a conventional quadrature-biased Mach Zehnder modulator (MZM) based FOL is around 100 dB·Hz$^{2/3}$ and is below the requirement for high performance applications such as cable TV and radar antenna remoting [1]. The SFDR of a link can be improved by suppressing the third order intermodulation distortion (IMD3) at $2\omega_1$-ω_2 and $2\omega_2$-ω_1 for a two-tone input with angular frequencies of ω_1 and ω_2.

The IMD3 in an externally modulated FOL is generated by the third and the higher odd order nonlinearity in the modulator transfer characteristic. It can be suppressed by eliminating the modulator third order nonlinearity and hence the link is linearized. The power of the IMD3 in a linearized FOL increases 5 dB for every dB increase in the input RF signal power. In this case, the IMD3 has a slope of 5, rather than 3 in an unlinearized FOL, when it is plotted against the input RF signal power [2], and the SFDR is dependent on the 4/5 power of the noise bandwidth.

Various linearization techniques with measured SFDRs ranged from 110 dB to 125 dB in a 1 Hz bandwidth have been reported [3–12]. Many of these techniques have the problem of the IMD3 can only be suppressed in a limited frequency range. This is due to precise control on the system parameter values is needed for IMD3 suppression and the frequency dependent characteristic of the electrical components used in the systems causes the system parameter

#347977 https://doi.org/10.1364/OE.27.004734
Journal © 2019 Received 12 Oct 2018; revised 12 Dec 2018; accepted 2 Jan 2019; published 8 Feb 2019

Optics EXPRESS

values to change as RF frequency changes. Techniques such as those without involving electrical components [8,9] and those using digital processing [6,12] have been proposed to overcome this problem. However, they have a complex structure, require expensive equipment or are only suitable for receiving channel. Furthermore, very few techniques have demonstrated a high SFDR performance can be achieved over a range of microwave frequency. For example, a high SFDR of around 125 dB in a 1 Hz bandwidth has been demonstrated over a 4-12 GHz frequency range using the feedforward linearization approach [13]. The drawbacks of this approach are that it involves optical-electrical-optical conversion and requires a matched fiber delay for synchronizing the baseband and distorted signal.

The aim of this paper is to present a simple all-optical linearized FOL. It is based on a dual-polarization modulator. The third order nonlinearity in the IMD3 is cancelled by optimizing the angle of a linear polarizer connected at the modulator output. Experimental results on an unamplified dual-polarization modulator based linearized FOL demonstrate a SFDR of more than 124 dB·Hz$^{4/5}$ in a 2-18 GHz frequency range. A high SFDR of 127.3 dB·Hz$^{4/5}$ is also demonstrated by using an optical amplifier to increase the average optical power into the photodetector.

2. Topology and principle of operation

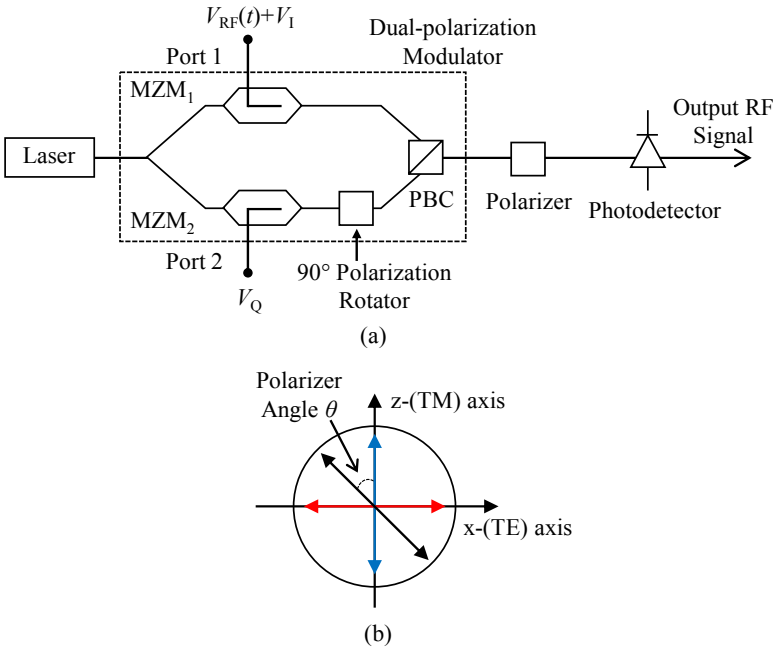

Fig. 1. (a) Topology of the dual-polarization modulator based linearized FOL. (b) The polarization states of the light passing though the top (↔) and bottom (↔) arm of the dual-polarization modulator and at the output of the polarizer (↔).

The structure of an all-optical linearized FOL is shown in Fig. 1(a). It consists of a laser, a commercial dual-polarization modulator, a linear polarizer and a photodetector. The linear polarized continuous-wave (CW) light travelled in the z-(TM) axis from a laser source is launched into the dual-polarization modulator, which is formed by two sub MZMs (MZM$_1$ and MZM$_2$) connected in parallel and a 90° polarization rotator connected after MZM$_2$. The RF signal and a bias voltage V_I are applied to Port 1 to modulate the optical carrier in MZM$_1$, which can be biased at the quadrature point for simplicity or close to the null point for optimizing the SFDR performance. MZM$_2$, which has no input RF signal, is biased at the

Optics EXPRESS

peak point to maximize the amplitude of the optical carrier passing through the modulator. The orthogonally polarized RF modulated optical signal and the unmodulated optical carrier are combined in a polarization beam combiner (PBC). They pass through a linear polarizer with an angle θ to the z-axis as shown in Fig. 1(b), which converts the two orthogonally linear polarized optical signals to have the same polarization state. Finally, the RF signal is recovered and the IMD3 is generated simultaneously after photodetection.

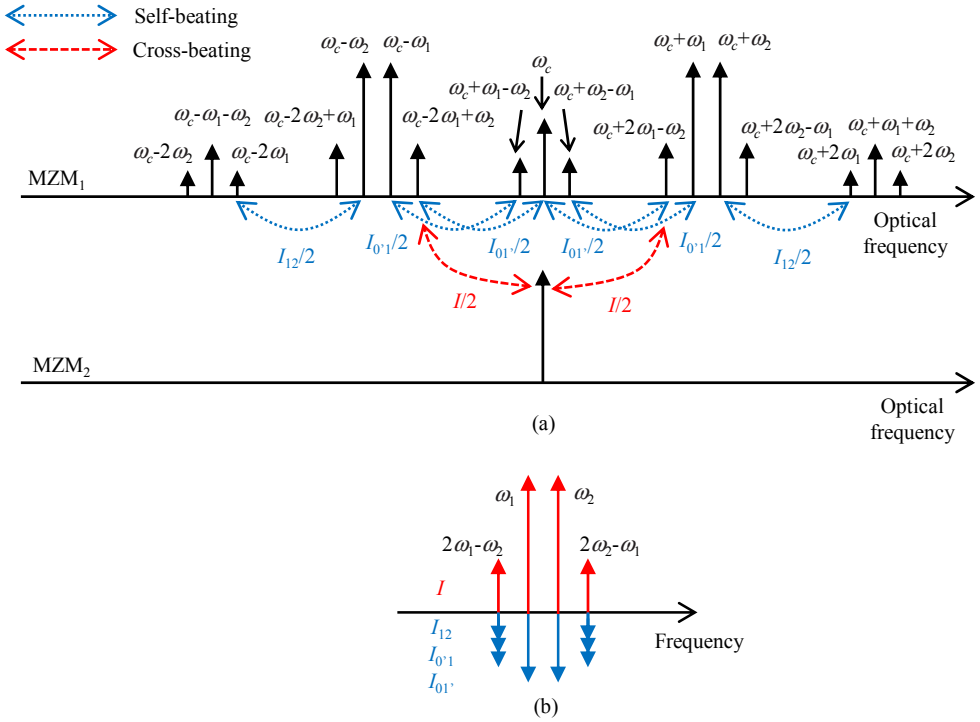

Fig. 2. (a) The optical spectrums at the linear polarizer output produced by the light passing through MZM$_1$ and MZM$_2$. (b) Photodetector output RF spectrum showing the RF signal and the IMD3 generated by beating between various frequency components.

The third order nonlinearity in the IMD3 generated by the structure shown in Fig. 1(a) can be cancelled via an optimum design of the polarizer angle θ. The principle is illustrated in Fig. 2. In a two-tone test, two RF signals with frequencies ω_1 and ω_2 are applied to MZM$_1$. Figure 2(a) shows the optical spectrums at the output of the linear polarizer for the light passing through MZM$_1$ and MZM$_2$. It can be seen that both the RF signal at ω_1 and ω_2 and the IMD3 at $2\omega_1$-ω_2 and $2\omega_2$-ω_1 can be generated by beating of the frequency components produced by MZM$_1$ itself at the photodetector, which is referred to as self-beating. They can also be generated by beating of the frequency components produced by MZM$_1$ and MZM$_2$ at the photodetector, which is referred to as cross-beating. The main contributors for IMD3 generation through self-beating and cross-beating are shown via the dotted lines and dashed lines in Fig. 2(a) respectively. Beating between various pairs of frequency components generate photocurrents at the IMD3 frequency of $2\omega_1$-ω_2, which are labelled as $I_{01'}$, $I_{0'1}$, I_{12} and I in Fig. 2. The figure shows the third order nonlinearity in the cross-beating IMD3 photocurrent I and the sum of the three self-beating IMD3 photocurrents $I_{01'}$, $I_{0'1}$ and I_{12} can be designed to have the same amplitude but opposite phase by optimizing the polarizer angle θ. This cancels the third order nonlinearity in the IMD3 of the FOL and consequently improves the SFDR performance. Note that optimizing the angle of a linear polarizer at the output of an optical phase modulator [14] and a MZM [15,16] to suppress the IMD3 have

Optics EXPRESS

been reported. However, they either only demonstrate IMD3 suppression without SFDR measurement [14,16] or show a limited measured SFDR of 105.5 dB·Hz$^{4/5}$ [15]. Furthermore, these previously reported polarization-based linearization techniques require the modulator to support both the TE and TM modes. The amplitudes of the light travelled in the TE and TM axes into the modulator also need to be accurately designed for IMD3 suppression. Using a dual-polarization modulator enables CW light travelled in the TM axis into the modulator to maximize the modulation efficiency as a conventional FOL, and most importantly its dynamic range performance is insensitive to change in the modulator input light polarization state.

3. Analysis

A two-tone RF signal with angular frequencies of ω_1 and ω_2 is applied to MZM_1. The electric fields at the output of MZM_1 and MZM_2 are given by [17]

$$E_{MZM_1,out} = \frac{\sqrt{2}}{4} E_{in} \sqrt{t_{ff}} e^{j\omega_c t} \left(e^{j(\beta_{RF}\sin(\omega_1 t)+\beta_{RF}\sin(\omega_2 t))} e^{j\beta_b} + \gamma e^{-j(\beta_{RF}\sin(\omega_1 t)+\beta_{RF}\sin(\omega_2 t))} e^{-j\beta_b} \right) \quad (1)$$

$$E_{MZM_2,out} = \frac{\sqrt{2}}{4} E_{in} \sqrt{t_{ff}} e^{j\omega_c t} (1+\gamma) \quad (2)$$

where E_{in} is the electric field amplitude of the CW light into the dual-polarization modulator, t_{ff} is the modulator insertion loss, ω_c is the angular frequency of the optical carrier, $\beta_{RF} = \pi V_{RF}/V_\pi$ is the modulation index, V_{RF} is the amplitude of the input RF signal, V_π is the half-wave voltage of MZM_1, $\beta_b = \pi V_1/V_\pi$ is the bias angle of MZM_1, $\gamma = \frac{\sqrt{\varepsilon}-1}{\sqrt{\varepsilon}+1}$ and ε is extinction ratio of the MZMs inside the dual-polarization modulator, which is defined as the ratio of maximum to minimum MZM output optical power. The extinction ratio is due to the losses in the two arms of the modulator are different [17]. We assume MZM_1 and MZM_2 have the same extinction ratio for simplicity. The 90° polarization rotator rotates the polarization state of the light at the output of MZM_2 by 90°. Hence the electric field at the output of the dual-polarization modulator can be written as

$$E_{out} = \frac{\sqrt{2}}{4} E_{in} \sqrt{t_{ff}} e^{j\omega_c t} \begin{Bmatrix} \left(e^{j(\beta_{RF}\sin(\omega_1 t)+\beta_{RF}\sin(\omega_2 t))} e^{j\beta_b} + \gamma e^{-j(\beta_{RF}\sin(\omega_1 t)+\beta_{RF}\sin(\omega_2 t))} e^{-j\beta_b} \right) \cdot \hat{z} \\ + (1+\gamma) \cdot \hat{x} \end{Bmatrix} \quad (3)$$

where $\hat{z}$ and $\hat{x}$ are the orthogonal polarization direction. The electric field at the output of the linear polarizer with an angle θ can be expressed as

$$E_{out,polarizer} = \frac{\sqrt{2}}{4} E_{in} \sqrt{t_{ff}} e^{j\omega_c t} \begin{Bmatrix} \begin{pmatrix} e^{j(\beta_{RF}\sin(\omega_1 t)+\beta_{RF}\sin(\omega_2 t))} e^{j\beta_b} \\ + \gamma e^{-j(\beta_{RF}\sin(\omega_1 t)+\beta_{RF}\sin(\omega_2 t))} e^{-j\beta_b} \end{pmatrix} \cdot \cos(\theta) \\ + (1+\gamma) \cdot \sin(\theta) \end{Bmatrix} \quad (4)$$

where θ is the polarizer angle to the z-axis. By using the Jacobi Anger expression

$$e^{ja\sin(\omega t)} = \sum_{n=-\infty}^{+\infty} J_n(a) e^{jn\omega t} \quad (5)$$

and considering all frequency components up to and including the second order sidebands in the linear polarizer output optical spectrum, Eq. (4) can be written as

Optics EXPRESS

$$E_{out,polarizer}=\frac{\sqrt{2}}{4}E_{in}\sqrt{t_{ff}}e^{j\omega_c t}\left\{\begin{array}{l}\left(\begin{array}{l}\left[\begin{array}{l}J_0(\beta_{RF})+J_1(\beta_{RF})e^{j\omega_1 t}+J_{-1}(\beta_{RF})e^{-j\omega_1 t}\\+J_2(\beta_{RF})e^{j2\omega_1 t}+J_{-2}(\beta_{RF})e^{-j2\omega_1 t}\end{array}\right]\\\cdot\left[\begin{array}{l}J_0(\beta_{RF})+J_1(\beta_{RF})e^{j\omega_2 t}+J_{-1}(\beta_{RF})e^{-j\omega_2 t}\\+J_2(\beta_{RF})e^{j2\omega_2 t}+J_{-2}(\beta_{RF})e^{-j2\omega_2 t}\end{array}\right]\cdot e^{j\beta_b}\\+\gamma\left[\begin{array}{l}J_0(\beta_{RF})-J_1(\beta_{RF})e^{j\omega_1 t}-J_{-1}(\beta_{RF})e^{-j\omega_1 t}\\+J_2(\beta_{RF})e^{j2\omega_1 t}+J_{-2}(\beta_{RF})e^{-j2\omega_1 t}\end{array}\right]\\\cdot\left[\begin{array}{l}J_0(\beta_{RF})-J_1(\beta_{RF})e^{j\omega_2 t}-J_{-1}(\beta_{RF})e^{-j\omega_2 t}\\+J_2(\beta_{RF})e^{j2\omega_2 t}+J_{-2}(\beta_{RF})e^{-j2\omega_2 t}\end{array}\right]\cdot e^{-j\beta_b}\end{array}\right)\cdot\cos(\theta)\\+(1+\gamma)\cdot\sin(\theta)\end{array}\right\} \quad (6)$$

where $J_n(x)$ is the Bessel function of nth order of the first kind. The output photocurrent I_{out} is the product of the photodetector responsivity $\Re$ and the output electric field amplitude squared, i.e.

$$I_{out}=E_{out,polarizer}\cdot E^{*}_{out,polarizer}\cdot\Re \quad (7)$$

The photocurrents at the RF signal frequency and the IMD3 frequency can be obtained by collecting the terms that contain ω_1 and $2\omega_1$-ω_2 from (7) respectively, and are given by

$$I_{out,RF}=-\frac{1}{2}E_{in}^2\Re t_{ff}\left\{\begin{array}{l}AB\sin(b-a)\cos^2(\theta)J_0(\beta_{RF})J_0(\beta_{RF})J_0(\beta_{RF})J_1(\beta_{RF})\\+B(1+\gamma)\sin(b)\sin(\theta)\cos(\theta)J_0(\beta_{RF})J_1(\beta_{RF})\end{array}\right\} \quad (8)$$

$$I_{out,IMD3}=-\frac{1}{2}E_{in}^2\Re t_{ff}\left\{\begin{array}{l}AB\sin(b-a)\cos^2(\theta)\left[\begin{array}{l}J_2(\beta_{RF})J_{-1}(\beta_{RF})J_0(\beta_{RF})J_0(\beta_{RF})\\+J_1(\beta_{RF})J_1(\beta_{RF})J_0(\beta_{RF})J_{-1}(\beta_{RF})\\+J_0(\beta_{RF})J_{-1}(\beta_{RF})J_0(\beta_{RF})J_2(\beta_{RF})\\+J_1(\beta_{RF})J_1(\beta_{RF})J_2(\beta_{RF})J_1(\beta_{RF})\\+J_3(\beta_{RF})J_1(\beta_{RF})J_0(\beta_{RF})J_1(\beta_{RF})\\+J_0(\beta_{RF})J_1(\beta_{RF})J_2(\beta_{RF})J_2(\beta_{RF})\\+.....\end{array}\right]\\+B(1+\gamma)\sin(b)\sin(\theta)\cos(\theta)J_2(\beta_{RF})J_{-1}(\beta_{RF})\end{array}\right\} \quad (9)$$

where the parameter A, B, a and b are the function of γ and β_b, and are given by

$$Ae^{ja}=\sqrt{\gamma^2+2\gamma\cos(2\beta_b)+1}\cdot e^{j\tan^{-1}\left[\tan(\beta_b)\frac{(1-\gamma)}{(1+\gamma)}\right]} \quad (10)$$

$$Be^{jb}=\sqrt{\gamma^2-2\gamma\cos(2\beta_b)+1}\cdot e^{j\tan^{-1}\left[\tan(\beta_b)\frac{(1+\gamma)}{(1-\gamma)}\right]} \quad (11)$$

The first three terms inside the square bracket in Eq. (9) are the three main contributors for IMD3 generation through self-beating, which generate the self-beating photocurrents ($I_{01'}$, $I_{0'1}$ and I_{12}) as indicated in Fig. 2. The latter three terms are the IMD3 generated by the self-beating between the frequency components in the higher order sidebands. Note that only the three main contributors for IMD3 generation through self-beating, and the IMD3 generated by cross-beating between the unmodulated optical carrier at ω_c in the bottom arm and the frequency components at ω_c+2ω_1–ω_2 and ω_c–2ω_1+ω_2 in the top arm, consist of the third order

Optics EXPRESS

nonlinearity. Therefore, the third order nonlinearity in the IMD3 of the dual-polarization modulator based FOL can be eliminated under the condition

$$AB\sin(b-a)\cos^2(\theta)\begin{bmatrix} J_2(\beta_{RF})J_{-1}(\beta_{RF})J_0(\beta_{RF})J_0(\beta_{RF}) \\ +J_1(\beta_{RF})J_1(\beta_{RF})J_0(\beta_{RF})J_{-1}(\beta_{RF}) \\ +J_0(\beta_{RF})J_{-1}(\beta_{RF})J_0(\beta_{RF})J_2(\beta_{RF}) \end{bmatrix} + B(1+\gamma)\sin(b)\sin(\theta)\cos(\theta)J_2(\beta_{RF})J_{-1}(\beta_{RF}) = 0 \quad (12)$$

Under small signal conditions, $J_0(\beta_{RF})\approx 1$, $J_1(\beta_{RF})\approx \beta_{RF}/2$ and $J_2(\beta_{RF})\approx \beta_{RF}^2/8$. Hence Eq. (12) can be written as

$$\tan(\theta) = -\frac{4A\sin(b-a)}{(1+\gamma)\sin(b)} \quad (13)$$

This shows a FOL based on a dual-polarization modulator and a linear polarizer can be linearized by simply adjusting the polarizer angle θ. Once the third order nonlinearity in the IMD3 has been cancelled, the fifth order nonlinearity from the six terms inside the square brackets in Eq. (9) becomes the dominant nonlinearity at the IMD3 frequency that limits the SFDR.

The output electrical powers at the RF signal frequency and the IMD3 frequency can be obtained from Eqs. (8) and (9), which are given by

$$P_{out,RF} = \frac{1}{8}P_{in}^2\Re^2 t_{ff}^2 R_o \left\{ \begin{matrix} AB\sin(b-a)\cos^2(\theta)J_0(\beta_{RF})J_0(\beta_{RF})J_0(\beta_{RF})J_1(\beta_{RF}) \\ +B(1+\gamma)\sin(b)\sin(\theta)\cos(\theta)J_0(\beta_{RF})J_1(\beta_{RF}) \end{matrix} \right\}^2 \quad (14)$$

$$P_{out,IMD3} = \frac{1}{8}P_{in}^2\Re^2 t_{ff}^2 R_o \left\{ \begin{matrix} AB\sin(b-a)\cos^2(\theta)\begin{bmatrix} J_2(\beta_{RF})J_{-1}(\beta_{RF})J_0(\beta_{RF})J_0(\beta_{RF}) \\ +J_1(\beta_{RF})J_1(\beta_{RF})J_0(\beta_{RF})J_{-1}(\beta_{RF}) \\ +J_0(\beta_{RF})J_{-1}(\beta_{RF})J_0(\beta_{RF})J_2(\beta_{RF}) \\ +J_1(\beta_{RF})J_1(\beta_{RF})J_2(\beta_{RF})J_1(\beta_{RF}) \\ +J_3(\beta_{RF})J_1(\beta_{RF})J_0(\beta_{RF})J_1(\beta_{RF}) \\ +J_0(\beta_{RF})J_1(\beta_{RF})J_2(\beta_{RF})J_2(\beta_{RF}) \\ +..... \end{bmatrix} \\ +B(1+\gamma)\sin(b)\sin(\theta)\cos(\theta)J_2(\beta_{RF})J_{-1}(\beta_{RF}) \end{matrix} \right\}^2 \quad (15)$$

where P_{in} is the CW light power into the dual-polarization modulator and R_o is the photodetector load resistance. Since there is no amplifier used in the link, the three fundamental noise components at the output of the dual-polarization modulator based linearized FOL are the laser intensity noise, the shot noise and the photodetector thermal noise [2]. The laser intensity noise and the shot noise are proportional to I_{avg}^2 and I_{avg} respectively, where I_{avg} is the average photocurrent and is given by

$$I_{avg} = \frac{1}{8}P_{in}\Re t_{ff}\left|Ae^{ja}\cos(\theta)J_0(\beta_{RF})J_0(\beta_{RF}) + \sin(\theta)(1+\gamma)\right|^2 \quad (16)$$

The SFDR of the dual-polarization modulator based linearized FOL is the difference between the output RF signal power given in Eq. (14) vertically downward to the point where the output IMD3 power given in Eq. (15) intersects with the total system output noise power. Note that the SFDR of the dual-polarization modulator based linearized FOL is dependent on MZM_1 bias angle β_b, the modulator extinction ratio ε and the polarizer angle θ. β_b and θ can

Optics EXPRESS

be optimized for a given modulator extinction ratio to maximize the SFDR performance of the link. The angle of the linear polarizer required to linearize the dual-polarization modulator based FOL for different MZM_1 extinction ratios can be found from Eq. (13) and is shown in Fig. 3. The simulation parameters are the relative intensity noise (RIN) of the optical source = −160 dB/Hz, P_{in} = 15.6 dBm, t_{ff} = 0.16, i.e. 8 dB modulator insertion loss, and $\Re$ = 0.7 A/W. The dashed line in Fig. 3 shows, for a given modulator extinction ratio, the angle of the polarizer required to eliminate the third order nonlinearity in the IMD3 and the corresponding SFDR when MZM_1 is biased at the quadrature point. It can be seen that the optimal polarizer angle is almost the same for different modulator extinction ratios. This is because the optical carrier at the output of a quadrature-biased MZM_1 dominates the residual carrier generated by the amplitude imbalance in the two arms of MZM_1. While biasing MZM_1 at the quadrature point is simple, only around 121 dB·$Hz^{4/5}$ SFDR can be obtained. The SFDR performance of the link can be improved by biasing MZM_1 close to the null point. Figure 4 shows the optimal bias angle of MZM_1 for a given modulator extinction ratio that results in the highest SFDR after linearization. The corresponding SFDR and the polarizer angle required to cancel the third order nonlinearity in the IMD3 are shown by the solid lines in Fig. 3. The results shown in these figures were obtained from Eqs. (13)-(16). Typical commercially available MZM has 30 dB extinction ratio. According to Fig. 4, if MZM_1 has 30 dB extinction ratio then the optimal modulator bias angle so that the link has the highest SFDR performance is 81.2°, which is 8.8° away from the null point. Under this condition, a linear polarizer with −30.9° angle to the z-axis is needed to linearize the dual-polarization modulator based FOL, which results in a high SFDR of 129.1 dB·$Hz^{4/5}$. The reason why a high SFDR can be obtained by low biasing MZM_1 is that the amplitude of the optical carrier is largely reduced compared to the case where MZM_1 is quadrature biased. This leads to a lower output average optical power and consequently lowers the system noise floor. At the same time, it has higher first order RF modulation sideband amplitude than that of the quadrature-biased MZM_1. The optimal polarizer angles for the dual-polarization modulator based linearized FOL when MZM_1 is biased at the quadrature point and close to the null point, have been simulated using the VPItransmissionMaker simulator. The results are in agreement with that obtained using Eq. (13), which verifies the correctness of the analysis.

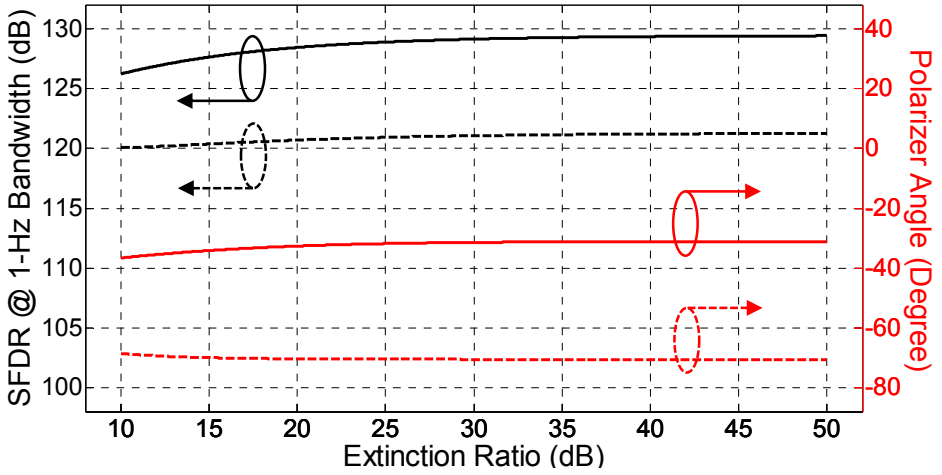

Fig. 3. The SFDR and the polarizer angle required to cancel the third order nonlinearity in the IMD3 versus the modulator extinction ratio when MZM_1 is biased at the quadrature point (dashed) and close to the null point that results in the highest SFDR (solid).

Optics EXPRESS

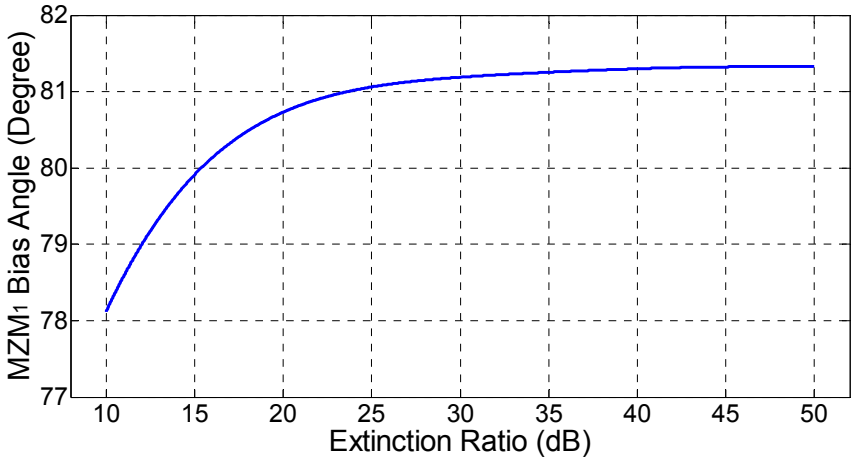

Fig. 4. Optimal bias angle of MZM_1 that results in the highest SFDR performance for the dual-polarization modulator based linearized FOL versus MZM_1 extinction ratio.

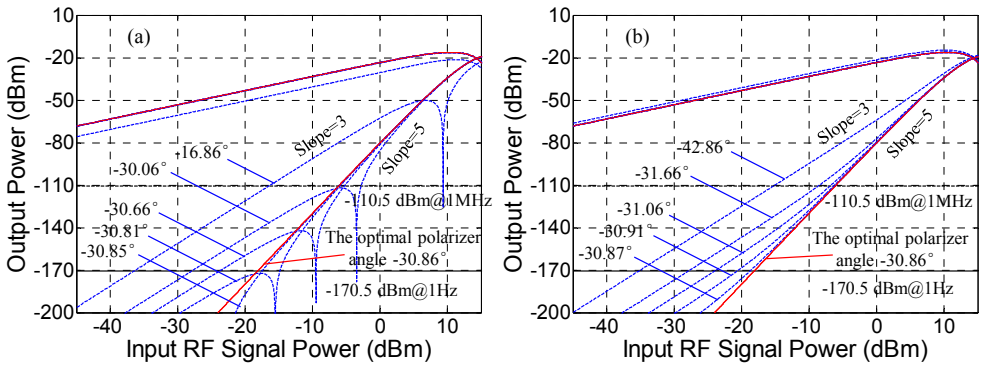

Fig. 5. Simulated dual-polarization modulator based linearized FOL output RF signal power, and IMD3 power for different polarizer angles. Also shown are the system output noise power for a 1 Hz noise bandwidth and a 1 MHz noise bandwidth. (a) Increasing the polarizer angle from the optimal value. (b) Decreasing the polarizer angle from the optimal value.

The effect of polarization sensitivity to the linearization technique was investigated. Figure 5 shows the simulated output RF signal power and IMD3 power together with the system noise power, for different polarizer angles. It can be seen that the SFDR degradation due to a small polarizer angle error is large for a very narrow noise bandwidth of 1 Hz. This is similar to that in a linearized FOL based on two MZMs connected in series with a modulator bias error [18]. However, in practice, the system noise bandwidth is much larger than 1 Hz. For example, for a 1 MHz noise bandwidth, the IMD3 slope remains around 5 even for a polarizer angle error of ± 0.8°. In this case, the SFDR is less sensitive to the polarizer angle. The proposed linearized FOL has a simple structure as it only involves a commercially available dual-polarization modulator and a linear polarizer. Most importantly the linearization process does not involve electrical components, which have frequency-dependent characteristic. Hence the link can be linearized over a very wide frequency range without the need of readjusting the system parameter values as the RF signal frequency changes. A polarizer with an optimum polarization angle to cancel the third order nonlinearity in the IMD3 can be integrated at the modulator output to form a single compact device, at the same time, to avoid change in SFDR performance due to movement. Commercial modulator

Optics EXPRESS

bias controllers, e.g. Plugtech MBC-NULL-03 bias controllers, have the ability to stabilize the modulator at around the null point [19]. This can be incorporated in the dual-polarization modulator based linearized FOL to maintain a high SFDR performance.

4. Experimental results

An experiment has been set up according to Fig. 1(a) to verify the broadband high SFDR capability of the dual-polarization modulator based linearized FOL. The optical source was a wavelength-tunable laser (Keysight N7711A), which was operated at a wavelength of 1550 nm and an optical power of 15.6 dBm. The optical modulator used in the experiment was a dual-polarization dual-drive modulator (Fujitsu FTM7980EDA). Two RF signals from microwave frequency generators passed through electrical isolators and combined via a power combiner. Since the two MZMs inside the dual-polarization modulator were dual-drive MZMs, the two-tone RF signal at the power combiner output was split by a 180° hybrid coupler before applied to the two input ports of MZM_1. The two RF ports of MZM_2 were terminated by 50 Ω terminators. The output of the dual-polarization modulator was connected to a polarization controller (PC) followed by an in-line polarizer, which blocks the light travelled in the fast axis of the fiber. They were functioned as a linear polarizer with an adjustable polarization angle. The output optical signal was detected by a photodetector (Discovery Semiconductors DSC30S). It had a typical responsivity of 0.8 A/W and a typical 1 dB small signal compression current of 16 mA. This shows the photodetector is operated in the linear region for less than 13 dBm input optical power. The photocurrent was fed into an electrical signal analyzer (Keysight N9000A) for measuring the power of the output RF signal and IMD3.

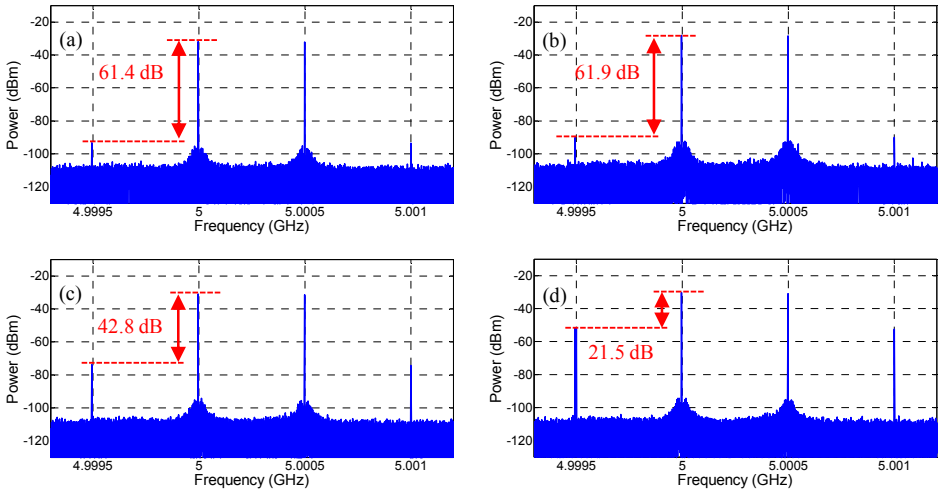

Fig. 6. Output electrical power of the dual-polarization modulator based linearized FOL when MZM_1 was biased (a) at the quadrature point and (b) close to the null point. Output electrical power of a conventional quadrature-biased MZM based FOL for (c) 2.5 dBm and (d) −0.7 dBm average optical power into the photodetector. The resolution bandwidth of the electrical signal analyzer was 10 Hz.

The bias voltage V_Q was adjusted to bias MZM_2 at the peak point. The frequencies of the two-tone RF signal into MZM_1 were 5 GHz and 5.0005 GHz, and MZM_1 was biased at the quadrature point. Note that the two frequency tones have a small separation of 0.5 MHz. This results in the output RF signal and IMD3 located in a small span of 1.5 MHz. Hence their powers can be measured in a short time even when both the electrical signal analyzer resolution and video bandwidths are 10 Hz. This setting lowers the noise floor displayed on the electrical signal analyzer, which allows the IMD3 power to be measured up to around

Optics EXPRESS

−110 dBm so that more data points can be obtained to improve the accuracy of the measured SFDR. Figure 6(a) shows the photodetector output electrical spectrum after adjusting the PC in front of the polarizer to suppress the IMD3. It can be seen that the output RF signal to IMD3 power ratio is 61.4 dB. The power of the two-tone RF signal into the dual-polarization modulator was varied and the corresponding output RF signal power and IMD3 power were measured as shown in Fig. 7(a). A 5 dB increase in the IMD3 power for 1 dB increase in the input RF signal power was obtained demonstrating the third order nonlinearity in the IMD3 was cancelled and hence the FOL was linearized. The average optical power into the photodetector was 2.5 dBm. The noise floor was measured by connecting a low noise amplifier with a gain of 26.3 dB after the photodetector to amplify the system noise floor to above the electrical signal analyzer noise floor. The noise floor shown on the electrical signal analyzer was −79.2 dBm for 1 MHz resolution bandwidth. This corresponds to −165.5 dBm in 1 Hz noise bandwidth without the low noise amplifier in the dual-polarization modulator based linearized FOL. The figure shows a measured SFDR of 119.9 dB·Hz$^{4/5}$. The polarizer angle for linearizing the FOL can be calculated based on the optical power measured before and after the polarizer together with Eq. (16). It was found to be −76.2°, which is close to the theoretical value of −70.5° shown in Fig. 3.

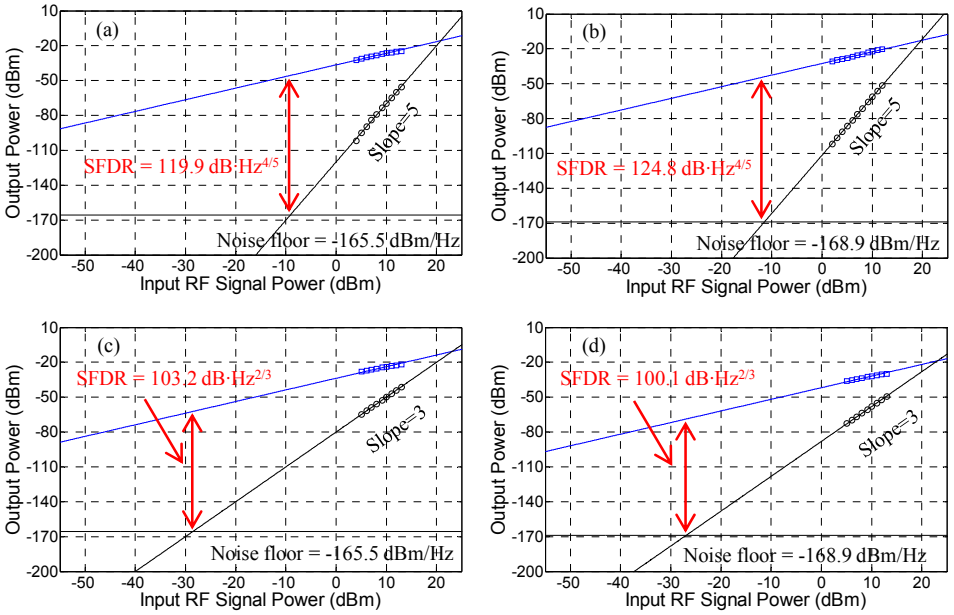

Fig. 7. Measured output RF signal power (square) and IMD3 power (circle) of the dual-polarization modulator based linearized FOL at different input RF signal powers when MZM_1 was biased (a) at the quadrature point and (b) close to the null point. The corresponding measurement for a conventional quadrature-biased MZM based FOL with (c) 2.5 dBm and (d) −0.7 dBm average optical power into the photodetector. The measured noise floor is −165.5 dBm/Hz and −168.9 dBm/Hz respectively.

The SFDR performance of the dual-polarization modulator based linearized FOL was also examined when the bias angle of MZM_1 was 85.6°, which is 4.4° away from the null point. The PC in front of the polarizer was adjusted to suppress the IMD3 amplitude. The photodetector output electrical spectrum is shown in Fig. 6(b). The output RF signal to IMD3 power ratio is 61.9 dB, which is similar to that when MZM_1 was biased at the quadrature point. The measured SFDR performance of the linearized FOL operating at the low-biased-MZM_1 mode is shown Fig. 7(b). The noise floor was measured to be −168.9 dBm/Hz for −0.7 dBm output average optical power. Hence an SFDR of 124.8 dB·Hz$^{4/5}$ was obtained.

Optics EXPRESS

A conventional FOL was set up by replacing the dual-polarization modulator in Fig. 1(a) with a quadrature-biased MZM (EOSPACE AX-OMSS), for comparison. In order to compare the output RF signal power to IMD3 power ratio between the two FOLs, the power of the laser source was adjusted so that the output average optical power was 2.5 dBm and –0.7 dBm, which are the same as that for the dual-polarization modulator based linearized FOL when MZM_1 is operating at the quadrature point and close to the null point. The input two-tone RF power was also adjusted to ensure the output RF power of the conventional FOL was the same as that in the dual-polarization modulator based linearized FOL. Figures 6(c) and 6(d) show the output electrical spectrums of the quadrature-biased MZM based FOL when the MZM was driven by a two-tone RF signal and the output average optical power are 2.5 dBm and –0.7 dBm respectively. The output RF signal to IMD3 power ratio is 42.8 dB and 21.5 dB, which are significantly smaller than that in the dual-polarization modulator based linearized FOL. The measured SFDR performance of the conventional FOL with 2.5 dBm and –0.7 dBm average optical power into the photodetector are shown in Figs. 7(c) and 7(d). It can be seen that, in both cases, since the MZM was not linearized, the power of the IMD3 increases by 3 dB for every dB increases in the input RF signal power. An SFDR of 103.2 $dB{\cdot}Hz^{2/3}$ and 100.1 $dB{\cdot}Hz^{2/3}$ was obtained from Figs. 7(c) and 7(d) respectively. This shows the dual-polarization modulator based linearized FOL operating in the quadrature- and low-biased-MZM_1 mode has a 16.7 dB and 24.7 dB SFDR improvement respectively compared to the conventional FOL based on a quadrature-biased MZM operating under the same condition.

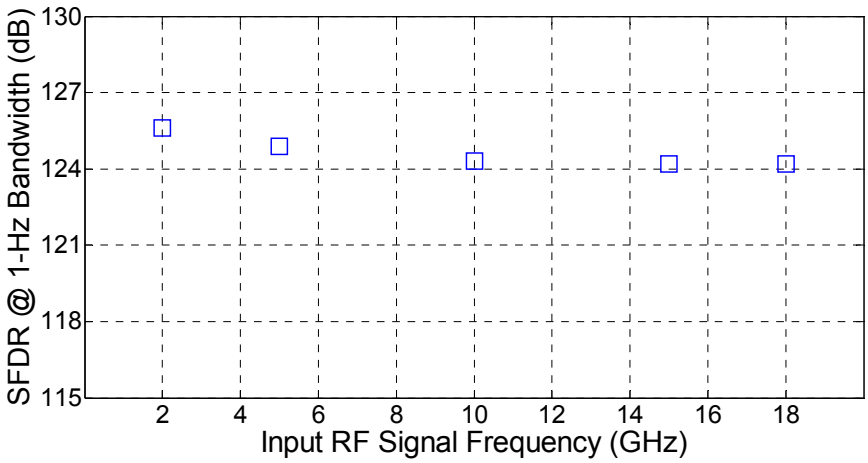

Fig. 8. The dual-polarization modulator based linearized FOL SFDRs measured at different input RF signal frequencies when MZM_1 was biased close to the null point.

In order to demonstrate the proposed linearized FOL has high SFDR performance at different input RF signal frequencies, MZM_1 inside the dual-polarization modulator was biased with a bias angle of 4.4° away from the null point as before. The PC in front of the polarizer was adjusted to suppress the IMD3. Figure 8 shows a high SFDR of more than 124 $dB{\cdot}Hz^{4/5}$ was obtained at different input RF signal frequencies over a wide frequency range from 2 GHz to 18 GHz without the need of readjusting the PC as the RF signal frequency changed. The result demonstrates the link remained linearized for different input RF signal frequencies due to no electrical components involved in the linearization process. There is less than 1.5 dB change in the SFDR measured at different input RF signal frequencies. The change is mainly due to the frequency dependent loss of the system. Note that the IMD3 power was stable throughout the SFDR measurement. Readjusting the PC in front of the linear polarizer to maintain IMD3 suppression was not required for the SFDR measurements

Optics EXPRESS

at different input RF signal frequencies. As was pointed out in Section 3, a linear polarizer with an optimal angle can be integrated at the output of the dual-polarization modulator to obtain robust SFDR performance when the system is used in practice.

Since the link was operated at a low output average optical power of −0.7 dBm, the shot noise was the highest noise component. Hence an erbium-doped fiber amplifier (EDFA) (Amonics AEDFA-PA-35) was used to increase the average optical power into the photodetector by 4.6 dB to 3.9 dBm. A 1 nm bandwidth optical filter centred at the laser wavelength was connected at the EDFA output to suppress the amplified spontaneous emission noise. In this case, the measured noise floor was increased by 5.1 dB to −163.8 dBm/Hz. Figure 9 shows an SFDR of 127.3 dB·Hz$^{4/5}$ was measured for 3.9 dBm output average optical power when MZM_1 inside the dual-polarization modulator was biased close to the null point. This shows a 3.2 dB SFDR improvement after using an EDFA to increase the output average optical power from −0.7 dBm to 3.9 dBm. The link gain, which is defined as the ratio of the output and input RF signal power, was also increased from −32.6 dB to −24.9 dB. Note that, as in most reported linearized FOLs [3–13], photodiode nonlinearity was not considered in the analysis. In other words, the analysis assumed a perfect linearized photodiode is used in the dual-polarization modulator based linearized FOL. In this case, the SFDR can be further increased by increasing the EDFA gain until the signal-spontaneous beat noise becomes the dominant noise source in the system. However, in practice, photodiodes are nonlinear devices like optical modulators, which generate IMD3s [20]. It was pointed out in [21] that the photodiode nonlinearity can set the upper limit on the SFDR in a FOL that consists of a linearized modulator. In order to minimize the effect of the photodiode nonlinearity on the SFDR, the EDFA only provided a gain of 4.6 dB so that the average optical power into the photodetector was 3.9 dBm. This corresponds to 2 mA photocurrent, which is well below the 1 dB small signal compression current of 16 mA specified in the photodetector datasheet. This shows the photodetector was operated in the linear region. It was difficult to obtain an IMD3 with a slope of 5 for a small input RF signal power in the SFDR measurement when the output average optical power was increased beyond 3.9 dBm. This could be due to the photodiode nonlinearity came into effect.

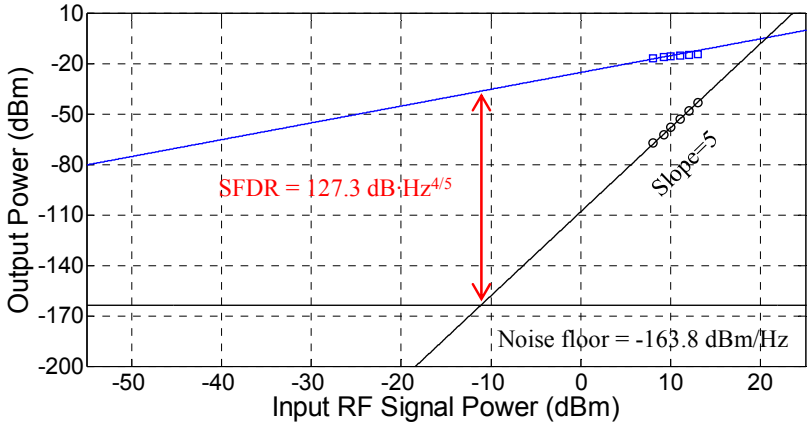

Fig. 9. Measured output RF signal power (square) and IMD3 power (circle) of the dual-polarization modulator based linearized FOL at different input RF signal powers when MZM_1 was biased close to the null point and an EDFA was used to increase the output average optical power to 3.9 dBm.

5. Conclusion

This paper has presented, for the first time that, using a commercial dual-polarization modulator to realize a broadband linearized FOL. The RF signal is applied to one of the

Optics EXPRESS

MZMs inside the dual-polarization modulator, which is biased either at the quadrature point for simplicity or close to the null point for optimizing the SFDR performance. The link is linearized by designing the angle of a linear polarizer connected after the dual-polarization modulator to cancel the third order nonlinearity in the IMD3. The link has a simple structure, and has inherently broad bandwidth as the RF signal is applied to only one MZM inside the dual-polarization modulator and the linearization process does not involve electrical components. The optimal polarizer angle in relation to the modulator extinction ratio has been analyzed and is in agreement with the VPItransmissionMaker simulation result. Experimental results have demonstrated a measured SFDR of more than 124 dB·Hz$^{4/5}$ at different input RF signal frequencies over a 2-18 GHz frequency range. With the use of an EDFA to increase the output average optical power to 3.9 dBm, a high SFDR of 127.3 dB·Hz$^{4/5}$ has been measured.

Funding

National Natural Science Foundation of China (NSFC) (61501205, 61771221).

References

1. C. Cox III, E. Ackerman, R. Helkey, and G. E. Betts, "Direct-detection analog optical links," IEEE Trans. Microw. Theory Tech. **45**(8), 1375–1383 (1997).
2. W. Chang, *RF photonic technology in optical fiber links*, (Cambridge University, 2002).
3. G. E. Betts and F. J. O'Donnell, "Microwave analog optical links using suboctave linearized modulators," IEEE Photonics Technol. Lett. **8**(9), 1273–1275 (1996).
4. W. B. Bridges and J. H. Schaffner, "Distortion in linearized electrooptic modulators," IEEE Trans. Microw. Theory Tech. **43**(9), 2184–2197 (1995).
5. Z. Chen, L. Yan, W. Pan, B. Luo, X. Zou, Y. Guo, H. Jiang, and T. Zhou, "SFDR enhancement in analog photonic links by simultaneous compensation for dispersion and nonlinearity," Opt. Express **21**(18), 20999–21009 (2013).
6. Y. Cui, Y. Dai, F. Yin, Q. Lv, J. Li, K. Xu, and J. Lin, "Enhanced spurious-free dynamic range in intensity-modulated analog photonic link using digital postprocessing," IEEE Photonics J. **6**(2), 1–8 (2014).
7. D. Zhu, J. Chen, and S. Pan, "Multi-octave linearized analog photonic link based on a polarization-multiplexing dual-parallel Mach-Zehnder modulator," Opt. Express **24**(10), 11009–11016 (2016).
8. E. I. Ackerman, G. E. Betts, and C. H. Cox, "Inherently broadband linearized modulator for high-SFDR, low-NF microwave photonic links," 2016 IEEE International Topical Meeting on Microwave Photonics (MWP) 265–268 (2016).
9. S. Li, X. Zheng, H. Zhang, and B. Zhou, "Highly linear radio-over-fiber system incorporating a single-drive dual-parallel Mach-Zehnder modulator," IEEE Photonics Technol. Lett. **22**(24), 1775–1777 (2010).
10. Y. Cui, Y. Dai, F. Yin, J. Dai, K. Xu, J. Li, and J. Lin, "Intermodulation distortion suppression for intensity-modulated analog fiber-optic link incorporating optical carrier band processing," Opt. Express **21**(20), 23433–23440 (2013).
11. D. Lam, A. M. Fard, and B. Jalali, "Digital broadband linearization of analog optical links," IEEE Photonics Conference 2012, 13149985 (2012).
12. P. Li, R. Shi, M. Chen, H. Chen, S. Yang, and S. Xie, "Linearized photonic IF downconversion of analog microwave signals based on balanced detection and digital signal post-processing," Proceedings of International Topical Meeting on Microwave Photonics, 68–71 (2012).
13. Y. Dai, X. Liang, F. Yin, J. Zhang, J. Li, W. Li, and K. Xu, "Feedforward linearization for RF photonic link with broadband adjustment-free operation," Opt. Express **25**(17), 20770–20779 (2017).
14. B. M. Haas and T. E. Murphy, "A simple, linearized, phase-modulated analog optical transmission system," IEEE Photonics Technol. Lett. **19**(10), 729–731 (2007).
15. B. Masella, B. Hraimel, and X. Zhang, "Enhanced spurious-free dynamic range using mixed polarization in optical single sideband Mach-Zehnder modulator," J. Lightwave Technol. **27**(15), 3034–3041 (2009).
16. B. Hraimel, X. Zhang, T. Liu, T. Xu, Q. Nie, and D. Shen, "Performance enhancement of an OFDM ultra-wideband transmission-over-fiber link using a linearized mixed-polarization single-drive x-cut Mach–Zehnder modulator," IEEE Trans. Microw. Theory Tech. **60**(10), 3328–3338 (2012).
17. H. Kim and A. H. Gnauck, "Chirp characteristics of dual-drive Mach-Zehnder modulator with a finite DC extinction ratio," IEEE Photonics Technol. Lett. **14**(3), 298–300 (2002).
18. G. E. Betts, "Linearized modulator for suboctave-bandpass optical analog links," IEEE Trans. Microw. Theory Tech. **42**(12), 2642–2649 (1994).
19. PlugTech Ultra High Precision MZM Bias Controller (MBC-NULL-03) data sheet. [Online]. Available: *www.plugtech.hk*.
20. N. J. Frigo, M. N. Hutchinson, and C. R. S. Williams, "Evaluating system penalties in radio frequency photonic links due to photodiode nonlinearity," Opt. Eng. **56**(10), 100501 (2017).

Optics EXPRESS

21. C. H. Cox III, E. I. Ackerman, G. E. Betts, and J. L. Prince, "Limits on the performance of RF-over-fiber links and their impact on device design," IEEE Trans. Microw. Theory Tech. **54**(2), 906–920 (2006).